Enhancing the Macroscopic Yield of Narrow-Band High-Order Harmonic Generation by Fano Resonances

Jan Rothhardt,[1,2,*] Steffen Hädrich,[1] Stefan Demmler,[1] Manuel Krebs,[1] Stephan Fritzsche,[2,3] Jens Limpert,[1,2] and Andreas Tünnermann[1,2,4]

[1]*Institute of Applied Physics, Abbe Center of Photonics, Friedrich-Schiller-Universität Jena, Albert-Einstein-Strasse 15, 07745 Jena, Germany*

[2]*Helmholtz-Institute Jena, Fröbelstieg 3, 07743 Jena, Germany*

[3]*Theoretisch-Physikalisches Institut, Friedrich-Schiller-Universität Jena, 07743 Jena, Germany*

[4]*Fraunhofer Institute of Applied Optics and Precision Engineering, Albert-Einstein-Strasse 7, 07745 Jena, Germany*

(Received 13 January 2014; revised manuscript received 28 February 2014; published 13 June 2014)

Resonances in the photoabsorption spectrum of the generating medium can modify the spectrum of high-order harmonics. In particular, window-type Fano resonances can reduce photoabsorption within a narrow spectral region and, consequently, lead to an enhanced emission of high-order harmonics in absorption-limited generation conditions. For high harmonic generation in argon it is shown that the $3s3p^6np^1P_1$ window resonances ($n = 4, 5, 6$) give rise to enhanced photon yield. In particular, the $3s3p^64p^1P_1$ resonance at 26.6 eV allows a relative enhancement up to a factor of 30 in a 100 meV bandwidth compared to the characteristic photon emission of the neighboring harmonic order. This enhanced, spectrally isolated, and coherent photon emission line has a relative energy bandwidth of only $\Delta E/E = 3 \times 10^{-3}$. Therefore, it might be very useful for applications such as precision spectroscopy or coherent diffractive imaging. The presented mechanism can be employed for tailoring and controlling the high harmonic emission of manifold target materials.

DOI: 10.1103/PhysRevLett.112.233002 PACS numbers: 32.30.−r, 42.50.Hz, 42.65.Ky

High harmonic generation (HHG) driven by a strong laser field represents an attractive method for generating coherent radiation in the extreme ultraviolet spectral region [1,2] and is, nowadays, widely employed in atomic, molecular, plasma, and solid state physics. In addition, HHG allows producing extremely short attosecond pulses, which enable ground-breaking investigations [3]. Typically, HHG suffers, however, from its inherently low conversion efficiency, which hinders applications that are especially dependent on a high photon flux.

In a simple single atom picture HHG can be described by a three-step model [4]: First, an electron tunnel ionizes through the atomic potential, which is modified by the strong laser field. Second, the electron propagates in the strong laser field. Finally, the electron may recombine with its parent ion and gives, thus, rise to the emission of a photon. In this picture, the power emitted by a single atom at the frequency ω_q is proportional to the square of the amplitude of the oscillating dipole $|A_q(t)|^2$, which is induced by the recombination process [4].

While the response of a single atom (A_q) is extremely small, phase matching of a large number of emitters gives rise to a coherent buildup of high-order harmonic (HH) emission along the propagation direction of the driving laser. By maximizing the number of phase-matched emitters, conversion efficiencies as high as of 4×10^{-4} have been achieved at 17 eV [5]. With the help of a simple model, which takes the emission of all emitters along the propagation axis, phase mismatch, and absorption into account, Constant *et al.* [6] found that the maximum conversion efficiency of HHG is ultimately limited by reabsorption of the generated HH photons within the generating medium itself. Furthermore, it was shown in Ref. [6], that this so-called absorption-limited conversion efficiency is proportional to $|A_q/\sigma_q|^2$, with σ_q being the absorption cross section at the harmonic frequency ω_q. Thus, the absorption-limited conversion efficiency of HHG can only be increased, by increasing the emission (A_q) or by reducing the reabsorption (σ_q) of HH photons.

So far, large efforts have been devoted to increasing A_q. For example, molecules [7] and noble gas clusters [8–10] have been employed as generating media.

Resonances involved in the generation process have also been explored for increasing the single-atom response A_q [11–13]. In particular, Ganeev *et al.* observed a significant resonant enhancement of a single harmonic order in indium plasma plumes [14,15] which they attribute to resonant transitions between autoionizing states and the ground state of singly charged transition metal ions. Their work inspired a number of theoretical and experimental studies about the physical nature of the enhancement process [16–19]. Recently, Strelkov [16] suggested an extension of the three-step model of HHG [4] in order to explain the experimentally observed enhancement: Instead of radiative recombination from continuum to the ground state, the free electron can also be trapped into an autoionizing state

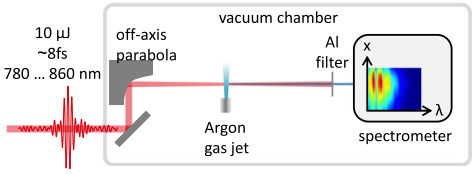

FIG. 1 (color online). Experimental setup for high harmonic generation: A few-cycle laser pulse, whose central wavelength is tunable between 780 and 860 nm, is focused upon an argon gas jet. An aluminum filter separates the fundamental laser radiation from the generated HH photons, which are analyzed spectrally and spatially by a grating-based spectrometer.

followed by a transition to the ground state and photon emission. If, particularly, the recombination via the autoionizing state has a larger probability than the direct recombination, an enhancement of HHG at the specific transition energy is to be observed.

Here, we report on the first experimental observation of resonant enhancement of high-order harmonics in argon. In particular, we analyze the underlying physical mechanism experimentally and suggest a simple model for its explanation. We conclude that in our case the resonant enhancement of the macroscopic HH emission is dominated by reduced absorption due to Fano resonances in the photoabsorption spectrum of the generation medium. Notably, the enhancement mechanism is of a different nature than what has previously been observed for various transition-metal ions [14,15].

The experiments are carried out using a few-cycle driving laser [20]. Owing to the large bandwidth supported by the laser system, its central wavelength can be tuned between 780 and 860 nm, with negligible changes in pulse duration (~8 fs), pulse energy (~10 μJ), and beam parameters. The experimental setup is illustrated in Fig. 1. An off-axis parabolic mirror is employed for focusing the laser pulses to a spot size of $2w_0 = 30$ μm, which enables a peak intensity of $\sim 2 \times 10^{14}$ W/cm^2. The target gas is provided by a 150 μm diameter nozzle. By placing the gas jet slightly behind the focus of the driving laser, phase matching of the short trajectories is achieved [21]. The fundamental radiation of the driving laser is blocked by a 200 nm thick aluminum filter, while the generated extreme ultraviolet (XUV) radiation is analyzed spatially and spectrally by means of a grating spectrometer. Since the XUV beam propagates freely in the spatial dimension parallel to the grating lines, spectrally resolved one-dimensional beam profiles can be recorded (energy resolution: $\Delta E/E = 2 \times 10^{-3}$).

Figure 2 displays a series of spectra that have been recorded with backing pressures between 1 and 9 bar and the central wavelength of the driving laser tuned to ~795 nm. At 1 bar (black) four distinct harmonic orders H15 to H21 are clearly observed. Because of the short pulse duration of our laser the individual harmonic orders appear as rather broad lines in the spectrum. At higher backing

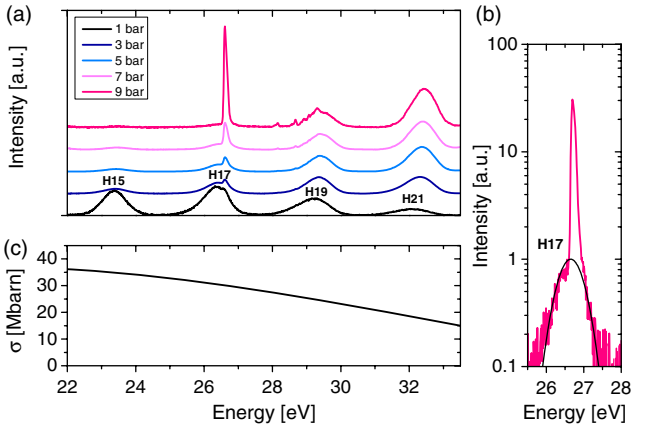

FIG. 2 (color online). (a) Spectra of high-order harmonics generated in argon at different backing pressures between 1 and 9 bar normalized to the peak of H19 at 29.2 eV (linear scale). At low pressure (black line) four harmonic orders (H15 to H21) are detected. As the pressure increases H15 and H17 are gradually suppressed due to absorption. Instead, a narrow but rather intense line occurs at 26.6 eV on top of H17 and a number of similar but weaker lines are observed between 29 and 30 eV. (b) Logarithmic plot of the spectrum around the strongest enhanced line at 26.6 eV measured at 9 bar (pink line) normalized to the peak of H17 (black line). (c) Measured continuous photoionization cross section reproduced from [22], which accounts for direct photoionization only without including any resonances.

pressures H15 and H17 are gradually suppressed. In addition, various narrow lines appear in the spectrum between 26 and 30 eV. A particularly strong and narrow line (FWHM ~0.1 eV, $\Delta E/E = 3 \times 10^{-3}$, Fourier-limited pulse duration ~23 fs) is observed at 26.6 eV and 9 bar (pink). This line is additionally shown on a logarithmic scale together with the underlying H17 in Fig. 2(b). Note that the peak intensity of this enhanced line (pink) is a factor of 30 higher than the peak of H17 which is represented by a Gaussian fit (black).

Figure 2(c) displays the continuous photoionization (PI) cross section measured by means of synchrotron radiation [22]. Since the photon energy is well above the ionization threshold, the PI cross section dominates the photoabsorption (PA) and represents the corresponding cross-section well. The strong suppression of the low-order harmonics (H15 and H17) at high backing pressures can be explained by the dramatic increase of the PA cross section from only 17 Mbarn at H21 to 35 Mbarn at H15.

The origin of the narrow lines that are observed at high backing pressure refers to a series of resonances involved in the PI cross sections of argon [23]. The enhanced lines observed in the HH spectra [Fig. 2(a)] clearly belong to the Fano resonances that have been observed in PI spectra by Madden *et al.* as displayed in Fig. 3(b) [23]. These resonances can be understood as interplay between the direct ionization and the photoexcitation of an inner subvalence electron to some Rydberg state, followed by a subsequent

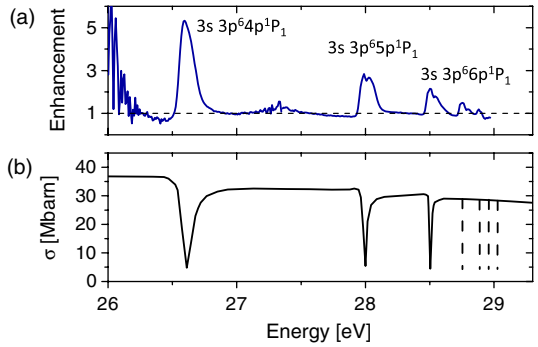

FIG. 3 (color online). (a) Spectral profiles of the observed resonances extracted from measurements of HH spectra at 7 bar. Each enhanced line is attributed to a transition from an autoionizing state to the ground state ($3S^2 3p^6$). (b) Photoionization cross section including the $3s3p^6np^1P_1$ series of window-type resonances measured by Madden *et al.* [23]. The dashed lines indicate the position of the nonresolved resonances with $n > 6$.

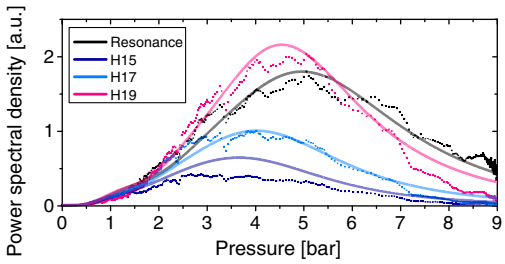

FIG. 4 (color online). Measured power spectral density at the center of H15 to H19 (dark blue, light blue, and pink dots) versus the applied backing pressure. The measured power spectral density at the center of the strongest resonant line (26.6 eV) involving the $3s3p^64p^1P_1$ state is shown as black dots. All values are normalized to the maximum obtained for H17. The semitransparent lines represent the result of a simulation.

autoionization process. Because of the different phases that are associated with these "quantum paths," the various shapes of isolated resonances can be described in terms of Fano profiles [24]. In the case of argon the autoionizing states of the $3s3p^6np^1P_1(n = 4, 5, 6)$ series result in so-called "window resonances," for which the direct and autoionization amplitudes virtually cancel each other and, hence, the PI cross section is dramatically reduced.

The measured HH spectra allow extracting the spectral line profiles of the observed resonances. To this end, an enhancement ratio has been introduced and is calculated as the photon signal in presence of the resonance divided by the expected signal without the resonance, which is found by a Gaussian fit to the underlying harmonic. The precision of this method has been maximized by tuning the peak of either H17 or H19 close to the resonance of interest by changing the wavelength of the driving laser (see the Supplemental Material [25]). Note the observed line profile of the resonance is not changed measurably by the driving laser wavelength. Figure 3(a) displays the extracted line profiles on top of the measured PI cross sections including the Fano resonances [Fig. 3(b)].

A number of experimental investigations have been carried out in order to prove that the enhanced radiation is coherent, has properties similar to the high-order harmonics and does not simply refer to spontaneous atomic line or plasma emission. First of all, the beam profile (Gaussian-like) and the divergence (half angle ~3 mrad) of the enhanced emission and the underlying harmonic are found to be identical (see Supplemental Material [25]). This proves directional emission, coupled to the wave front of the driving laser. Second, at low backing pressures a quadratic increase of the signal with backing pressure is observed for both the enhanced lines and the neighboring harmonics indicating coherent emission of an increasing number of emitters.

This pressure dependence is illustrated in Fig. 4. The dots represent the measured power at the center of H15 (dark blue), H17 (light blue), H19 (pink), and the line enhanced by the $3s3p^64p^1P_1$ resonance (black) versus backing pressure. It can be seen that H15, H17, and H19 peak at about 3.5, 4, and 4.5 bar, respectively. However, the enhanced line increases until 5 bar and decreases much slower than the harmonics when the backing pressure is further increased. The estimated conversion efficiency (see Supplemental Material [25]) into a 0.1% bandwidth is 8×10^{-8} for H17 at 4 bar while it is enhanced by a factor of ~1.8 to 1.5×10^{-7} for the resonant line at 5 bar which corresponds to $\sim 1.3 \times 10^{10}$ photons/s.

To investigate the effects of different backing pressure on phase matching and absorption we employ the model introduced in Ref. [6]. The number of photons emitted on axis into the qth harmonic per unit of time and area can be calculated as [6,26]

$$N_{\mathrm{out}} \sim \rho^2 A_q^2 \frac{4L_{\mathrm{abs}}^2}{1 + 4\pi^2 (L_{\mathrm{abs}}^2 / L_{\mathrm{coh}}^2)} \times \left[1 + \exp\left(-\frac{L_{\mathrm{med}}}{L_{\mathrm{abs}}}\right) - 2\cos\left(\pi \frac{L_{\mathrm{med}}}{L_{\mathrm{abs}}}\right) \times \exp\left(-\frac{L_{\mathrm{med}}}{2L_{\mathrm{abs}}}\right)\right], \quad (1)$$

when A_q and the gas density ρ are assumed to be constant within the generating volume. The pressure dependent absorption length $L_{\mathrm{abs}} = 1/\rho\sigma_q$ is calculated via the measured continuous PI cross sections of argon [22]. The target pressure p and, consequently, the density ρ in the interaction region is calculated to be about 40% of the backing pressure, if we assume that the center of the laser beam is as close as 30 μm ($2w_0$) to the nozzle opening [27]. The coherence length $L_{\mathrm{coh}} = \pi/\Delta k$ is determined by the phase mismatch Δk, which is calculated as the difference between a pressure-independent Gouy phase term Δk_{Gouy}

and the pressure dependent dispersion of the gas atoms $\Delta k_{\mathrm{Disp}} = (p/p_0)(2\pi/\lambda_0)\Delta$. Here, p_0 is the standard pressure (1013 mbar), λ_0 is the driving laser wavelength, and $\Delta\delta$ is the refractive index difference between fundamental and harmonic taken from [28]. Negligible ionization and dipole phase [21] is assumed.

Because of the characteristics of the utilized vacuum pump, the density of residual gas in the vacuum chamber is proportional to the backing pressure. The constant phase mismatch term $\Delta k_{\mathrm{Gouy}}(1.3 \times 10^5\ \mathrm{m}^{-1})$ and the density length product of the additional absorbing atoms (residual gas) have been used as fit parameters to best match the experiment. The latter one is found to be 6 $\mu\mathrm{m}\sigma_0\ p_{\mathrm{back}}/\mathrm{bar}$, which is a factor of 10 lower than the density length product within the gas jet. Consequently, most of the absorption is located in the generating medium itself.

The results of the simulation are displayed as semitransparent lines in Fig. 4 (dark blue, light blue, and pink). The pressure dependence of the resonant line at 26.6 eV can be reproduced by the model as well (black line), if the refractive index difference $\Delta\delta$ is reduced by 15%. We assume that this originates from an additional phase related to the resonance. Furthermore, the effective absorption cross section is determined to be $25 +/- 1$ Mbarn, which is significantly lower compared to the background cross section of 30 Mbarn that has been measured at this energy [22]. Hence, the model strongly supports our interpretation of reduced absorption due to the resonance.

In a second step, the model is employed to investigate the spectral characteristics of the resonance. The HH orders are well reproduced by representing each harmonic order in $A_q(\omega)$ with a Gaussian profile of adequate width. Within the spectral region of interest we assume $\Delta\delta$ to be constant and neglect additional phases due to the resonance. In addition, the absorption cross section was modeled by including the strongest resonance using Fano's parametrization [24]. Here, the resonance energy and width as well as the q parameter and correlation index (that describe the shape and the strength of the resonance) have been used as fit parameters. The simulated emission spectrum was corrected by the spectrometer resolution and agrees remarkably well with the measured spectrum [see Fig. 5(a)]. The corresponding effective absorption cross section is shown in Fig. 5(b). The effective half-width of the $3s3p^6 4p^1P_1$ resonance in our experiment is found to be $\Gamma = 0.18$ eV, the correlation index is $\rho^2 = 0.175$, and the q factor is $q = -0.55$. These values differ from what has been measured in PI with synchrotron radiation ($\Gamma = 0.08$ eV,$\rho^2 = 0.86$, and $q = -0.22$) [23] Most obviously, a minimum cross section of 25 Mbarn is obtained, 5 times larger than found in [23]. These differences can be attributed to the fact that the resonances are influenced by the strong laser field. While time-resolved absorption measurements have already unveiled a laser-induced spectral shift, weakening and line splitting of the involved resonances [29], here we observe a

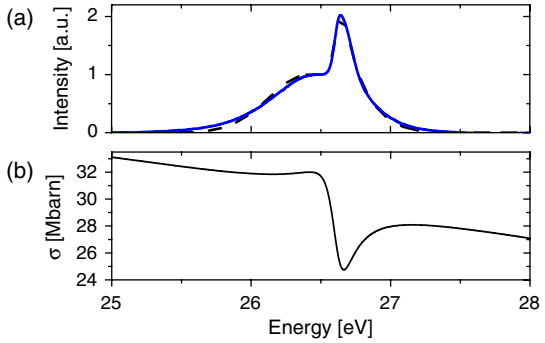

FIG. 5 (color online). Zoom into the spectral region containing only H17 and the $3s3p^6 4p - 3S^2 3p^6$ resonance at 26.6 eV. (a) Measured spectrum at 5 bar (blue line) and spectrum calculated from a corresponding simulation (black dashed line). (b) Absorption cross section used for calculating the spectrum presented on top. A Fano resonance profile has been added to the measured direct photoionization cross section taken from [22] and the effective width; the q factor and correlation index have been chosen to match the experimental result best.

time-averaged response of the absorbing medium resulting in broadened and weakened resonance lines. Note that such Fano resonances, in particular, the relative phase of the interfering channels, can also be controlled by laser pulses [30]. This holds promise for controlling the harmonic emission and resonant enhancement in the spectral and time domain by an additional pulse. The presented mechanism is universal and is expected to be observable in many other target materials. Indeed, our setup allows observing a significant enhancement of a narrow spectral line due to the $4s4p^6 5p^1P_1$ window resonance at 25 eV in krypton. Furthermore, we observed suppression of three narrow spectral lines between 45 and 47.2 eV in neon, due to resonances involving the $2p^4 3s3p^1P_1$, $2s2p^6 3p^1P_1$, or $2s2p^6 4p^1P_1$ states, which lead to increased absorption [31]. Similar resonances involving autoionizing states have been faintly observed by HHG in helium [32], are known for xenon [33] and can be found in many other multielectron systems.

The enhanced narrow line(s) in the HH spectrum of argon at high backing pressure can be understood by the (window) resonances in the PI spectrum. At low backing pressure, in contrast, no resonances are observed in the HH spectra, indicating that the single-atom response is not affected by the resonances (see discussion in the Supplemental Material [25]). Hence, in the presence of autoionizing resonances, photorecombination cannot be treated as inverse PI anymore as usually assumed [34].

In summary, we demonstrate that resonances in the photoabsorption spectrum of the generating medium can significantly affect and modify the spectrum of high-order harmonics under absorption-limited conditions. First experiments in argon show that window resonances due to the virtual excitation of autoionizing states give rise to

enhanced macroscopic photon emission. In particular, the $3s3p^6 4p^1P_1$ resonance at 26.6 eV reduces reabsorption and, therefore, allows enhancing the conversion efficiency by a factor of 1.8 within a narrow spectral region. At highest backing pressure, this narrow line is further enhanced up to a factor of 30 relative to the underlying HH and possesses a relative energy bandwidth of only $\Delta E/E = 3 \times 10^{-3}$. This makes it very attractive for applications requiring narrowband XUV radiation.

The presented mechanism provides a simple and easy to implement way of tailoring and enhancing high harmonic emission and can be applied to a huge variety of targets. In combination with high average power driving lasers [35] it will enable tabletop XUV sources of unprecedented brightness and spectral purity. Thus, applications such as precision spectroscopy of highly charged ions [36] or coherent diffractive imaging of nanoscale objects with unprecedented level of detail [37] will be feasible in the future.

This work has been supported by the German Federal Ministry of Education and Research (BMBF) and the European Research Council (FP7/2007-2013)/ERC Grant Agreement No. 240460. We thank Pascal Salières for fruitful discussions.

*Corresponding author.j.rothhardt@gsi.de

[1] M. Ferray, A. L'Huillier, and X. Li, J. Phys. B **21**, L31 (1988).
[2] A. McPherson, G. Gibson, H. Jara, U. Johann, T. S. Luk, I. A. McIntyre, K. Boyer, and C. K. Rhodes, J. Opt. Soc. Am. B **4**, 595 (1987).
[3] F. Krausz and M. Ivanov, Rev. Mod. Phys. **81**, 163 (2009).
[4] P. B. Corkum, Phys. Rev. Lett. **71**, 1994 (1993).
[5] E. Takahashi, Y. Nabekawa, and K. Midorikawa, Opt. Lett. **27**, 1920 (2002).
[6] E. Constant, D. Garzella, P. Breger, E. Mével, C. Dorrer, C. Le Blanc, F. Salin, and P. Agostini, Phys. Rev. Lett. **82**, 1668 (1999).
[7] C. Lynga, A. L'Huillier, and C.-G. Wahlström, J. Phys. B **29**, 3293 (1996).
[8] T. D. Donnelly, T. Ditmire, K. Neuman, M. D. Perry, and R. W. Falcone, Phys. Rev. Lett. **76**, 2472 (1996).
[9] J. W. G. Tisch, T. Dittmire, D. J. Fraser, N. Hay, M. B. Mason, E. Springate, J. P. Marangos, and M. H. R. Hutchinson, J. Phys. B **30**, L709 (1997).
[10] H. Ruf, C. Handschin, R. Cireasa, N. Thiré, A. Ferré, S. Petit, D. Descamps, E. Mével, E. Constant, V. Blanchet, B. Fabre, and Y. Mairesse, Phys. Rev. Lett. **110**, 083902 (2013).
[11] E. S. Toma, P. Antoine, A. de Bohan, and H. G. Muller, J. Phys. B **32**, 5843 (1999).
[12] M. Barkauskas, F. Brandi, F. Giammanco, D. Neshev, a. Pirri, and W. Ubachs, J. Electron Spectrosc. Relat. Phenom. **144–147**, 1151 (2005).
[13] P. Ackermann, H. Münch, and T. Halfmann, Opt. Express **20**, 13824 (2012).
[14] R. A. Ganeev, M. Suzuki, M. Baba, H. Kuroda, and T. Ozaki, Opt. Lett. **31**, 1699 (2006).
[15] R. A. Ganeev, P. A. Naik, H. Singhal, J. A. Chakera, and P. D. Gupta, Opt. Lett. **32**, 65 (2007).
[16] V. Strelkov, Phys. Rev. Lett. **104**, 123901 (2010).
[17] M. Tudorovskaya and M. Lein, Phys. Rev. A **84**, 013430 (2011).
[18] S. Haessler, L. B. E. Bom, O. Gobert, J.-F. Hergott, F. Lepetit, M. Perdrix, B. Carré, T. Ozaki, and P. Salières, J. Phys. B **45**, 074012 (2012).
[19] S. Haessler, V. Strelkov, L. B. Elouga Bom, M. Khokhlova, O. Gobert, J.-F. Hergott, F. Lepetit, M. Perdrix, T. Ozaki, and P. Salières, New J. Phys. **15**, 013051 (2013).
[20] J. Rothhardt, S. Demmler, S. Hädrich, J. Limpert, and A. Tünnermann, Opt. Express **20**, 10870 (2012).
[21] M. Lewenstein, P. Salieres, and A. L'Huillier, Phys. Rev. A **52**, 4747 (1995).
[22] G. Marr and J. West, At. Data Nucl. Data Tables **18**, 497 (1976).
[23] R. P. Madden, D. L. Ederer, and K. Codlin, Phys. Rev. **177**, 136 (1969).
[24] U. Fano, Phys. Rev. **124**, 1866 (1961).
[25] See the Supplemental Material at http://link.aps.org/supplemental/10.1103/PhysRevLett.112.233002 for spectra that have been recorded with different driving laser wavelengths, beam profiles of the XUV emission, and a detailed discussion on the difference in photoionization and photorecombination in presence of autoionizing resonances.
[26] S. Kazamias, D. Douillet, F. Weihe, C. Valentin, A. Rousse, S. Sebban, G. Grillon, F. Augé, D. Hulin, and P. Balcou, Phys. Rev. Lett. **90**, 193901 (2003).
[27] D. R. Miller, *Atomic Molecular Beam Methods* (Oxford University Press, Oxford, 1988).
[28] B. L. Henke, E. M. Gullikson, and J. C. Davis, At. Data Nucl. Data Tables **54**, 181 (1993).
[29] H. Wang, M. Chini, S. Chen, C.-H. Zhang, F. He, Y. Cheng, Y. Wu, U. Thumm, and Z. Chang, Phys. Rev. Lett. **105**, 143002 (2010).
[30] C. Ott, A. Kaldun, P. Raith, K. Meyer, M. Laux, J. Evers, C. H. Keitel, C. H. Greene, and T. Pfeifer, Science **340**, 716 (2013).
[31] K. Schulz, M. Domke, R. Püttner, a Gutiérrez , G. Kaindl, G. Miecznik, C. Greene, Phys. Rev. A **54**, 3095 (1996).
[32] S. Gilbertson, H. Mashiko, C. Li, E. Moon, and Z. Chang, Appl. Phys. Lett. **93**, 111105 (2008).
[33] D. L. Ederer, Phys. Rev. A **4**, 2263 (1971).
[34] A.-T. Le, R. Lucchese, S. Tonzani, T. Morishita, and C. Lin, Phys. Rev. A **80**, 013401 (2009).
[35] S. Hädrich, M. Krebs, J. Rothhardt, H. Carstens, S. Demmler, J. Limpert, and A. Tünnermann, Opt. Express **19**, 19374 (2011).
[36] W. Nörtershäuser, Hyperfine Interact. **199**, 131 (2011).
[37] M. D. Seaberg, D. E. Adams, E. L. Townsend, D. A. Raymondson, W. F. Schlotter, Y. Liu, C. S. Menoni, L. Rong, C.-C. Chen, J. Miao, H. C. Kapteyn, and M. M. Murnane, Opt. Express **19**, 22470 (2011).